Advanced Composite Materials
Publication details, including instructions for authors and subscription information:
http://www.tandfonline.com/loi/tacm20

Prediction of the stiffness degradation in cross-ply laminates due to transverse matrix-cracking: an energy method approach

R. Anderssen [a] , P.A. Gradin [b] & C.G. Gustafson [c]

[a] Department of Machine Design and Material Technology, Norwegian University of Science and Technology, N-70:34 Trondheim, Norway

[b] Department of Machine Design and Material Technology, Norwegian University of Science and Technology, N-70:34 Trondheim, Norway

[c] Department of Machine Design and Material Technology, Norwegian University of Science and Technology, N-70:34 Trondheim, Norway

Version of record first published: 02 Apr 2012.

To cite this article: R. Anderssen , P.A. Gradin & C.G. Gustafson (1998): Prediction of the stiffness degradation in cross-ply laminates due to transverse matrix-cracking: an energy method approach, Advanced Composite Materials, 7:4, 325-346

To link to this article: http://dx.doi.org/10.1163/156855198X00237

Adv. Composite Mater., Vol. 7, No. 4, pp. 325–346 (1998)

Prediction of the stiffness degradation in cross-ply laminates due to transverse matrix-cracking: an energy method approach

R. ANDERSSEN, P. A. GRADIN and C. G. GUSTAFSON*

Department of Machine Design and Material Technology, Norwegian University of Science and Technology, N-7034 Trondheim, Norway

Received 25 March 1998; accepted 19 June 1998

Abstract—This study deals with transverse cracking in cross-ply laminates. A fracture mechanics analysis, using a strain energy based criterion, was used to model the onset of transverse matrix cracking, and the conditions for further damage development. An admissible displacement field, involving unknown functions was assumed, and the principle of minimum potential energy was used to establish these functions. The crack front shape was a part of the assumed displacement field, thus making it possible to minimise the strain energy with respect to the crack opening displacement function. In this paper the aim was to establish a solution to the transverse cracking problem, to use later in a numerical procedure for the viscoelastic damage predictions for a cross-ply laminate. The model accounts for residual stresses. A number of finite element solutions were performed to verify the accuracy of the presented analytical solution. Predictions of stiffness degradation due to matrix cracking, and matrix cracking as a function of applied stress are presented.

Keywords: Damage mechanics; transverse cracking; energy methods; stiffness degradation; cross-ply composites; residual stresses.

1. INTRODUCTION

The damage process of advanced high-performance composites is rather complex, and consists of a variety of damage modes due to the heterogeneity of the composite. Types of damage can be matrix cracking (intra-laminar), debonding between fibre and matrix, or fibre fracture and delamination (inter-laminar) between plies. Normally, the first mode of damage in cross-ply and angle-ply laminates is matrix cracking in the off-axis plies, with cracks following the fibre direction. Matrix cracks are observed during short and long term static, fatigue, and thermal loading,

*To whom correspondence should be addressed.

or any combination of these load cases. The formation of matrix cracks often have a relatively minor effect on the mechanical properties for very low crack densities, but may have a large effect on the mechanical [1] and physical [2] properties of the composite, as the crack density increases. Another undesirable effect is fluid following the cracks through the laminate. One example is weeping in pipes and leakage in pressure vessels, that might lead to catastrophic failure and environmental hazards. The penetration of fluids in the composite can alter the long-term properties and the all-over behaviour of the composite. Even if matrix cracks can be tolerated in many applications for low crack densities, there might be cases where these cracks act as starting points for further and more serious damage modes [3].

The occurrence of micro-cracking in fibre reinforced composite laminates has resulted in numerous scientific studies covering this phenomenon. The analysis of the increase in transverse cracks in a structure was initiated with the works of Reifsnider [4] and Garret and Bailey [5]. They were the first to show that the crack density increased monotonically, and reaches a saturation limit with a practically uniform crack spacing. Bader *et al.* [3] and Wang *et al.* [6, 7] demonstrated the dependence of initiation of the first crack and its multiplication on the thickness of the cracked structure. It then became essential to understand, and to be able to model, the cracking process and the damage mechanisms. There has been extensive research on the mathematical modelling of degradation of mechanical and physical properties in laminated composites, due to transverse matrix cracks. It is possible to divide these models into different types, depending on the approach used.

1.1. Continuum damage mechanics

The total set of failure entities is termed as damage, and the failure entities of the same orientation and same growth characteristics are grouped in one damage mode. To each damage mode, a vector or a tensor field quantity is assigned. This quantity represents an average effect of all failure entities of that mode, in a representative volume element. Talreja [8] and Allen *et al.* [9], were the first to apply this approach to the matrix cracking problem. Allen *et al.* generalise all damage states into a damage tensor. The most significant difference is that the damage, (ISV, the internal state variable), in Talreja's first model is a vector, and in Allen's model a second order tensor. Renard and Thionnet [10] introduced a scalar damage variable to describe the transverse cracking. For continuum damage mechanics approaches, the composite is then treated as a continuum, and one seeks to find constitutive relations between stress, strain and damage. For the application of these methods, a set of unknown damage constants must be determined experimentally, and the method does not provide either stress or strain distributions in the cracked layer. It uses no fracture mechanics or crack propagation theories, and therefore does not make any prediction about damage propagation.

1.2. Shear-lag models

Several shear-lag models [4, 5, 11–14] have been presented, based on different assumptions. Garret and Bailey [5] presented a shear stress transfer coefficient, while Reifsnider [4], and Laws and Dworak [11] were the first to introduce a shear stress transfer layer. Physically, most of the approaches are to introduce a shear stress transfer layer. The far-field tensile stress is transferred to the cracked layer, via shear deformation of the thin boundary layer at the layer interface. The procedure for shear-lag analysis is relatively simple, and results in a reasonably accurate prediction of the stiffness reduction as a function of crack density. These methods give good results when compared to experimental data, but suffer from lack of generality, because it is not clear how to determine the boundary layer thickness in a systematic way. The major disadvantage of this approach is that the shear stiffness of the shear transfer layer is an unknown parameter, that must be determined by fitting to experimental results.

1.3. Energy methods

These models are based on the principle of minimum potential or minimum complementary energy, respectively. Hashin [15, 16] used the principle of minimum complementary energy to calculate out-of-plane stresses and effective stiffness. Hashin makes only on one assumption, saying that the x-axis tensile stresses in each ply depend only x, and are independent of the thickness coordinate. Nairn *et al.* [17, 18] extend the Hashin solution to also account for residual stresses. Several authors have used the same principles as Hashin, but modified the assumptions on the assumed stress field. Varna *et al.* [19] introduce a non-uniform stress distribution in the layers, and also accounts for residual stresses. Nairn and Hu [20] state that the improvement of Hashin's analysis over the best one-dimensional analysis is only marginal. Fang *et al.* [21] assumed a displacement field, and derived a variational solution by minimising the potential energy, but they assume zero displacement in the thickness direction, which results in a one-dimensional analysis. The accuracy of these approaches, however, depends on the assumptions made regarding the stress or the displacement fields of each layer.

2. FRACTURE MECHANICS ANALYSIS

In the present work, several assumptions are made regarding the crack propagation. It has been found that the first phase of damage development in a composite laminate is matrix cracking, with increasing crack density during loading, which is typified by development of a characteristic damage state (CDS), composed primarily of matrix cracking in off-axis plies. For the current model, it is assumed that the crack spacing is uniform, and that the crack density reaches a saturation limit, the characteristic damage state. Only straight (no curved or oblique) microcracks

are considered and no crack-tip delamination is accounted for, although these phenomena have been observed in experiments [5, 21]. All laminates have inherent processing flaws, and some of these flaws can initiate microcracks at lower strains than expected. Varna and Berglund [25] have studied the crack propagation in both width and thickness directions, and discussed the flaw size effects on the propagation. Although the inherent material microflaws may be considered to exist randomly in the laminate, the general characteristics of the macroscopic matrix cracks are found to be highly dependent on the lamination geometry, such as laminae stacking sequence and lamina thickness. Thus for a given laminate under a given loading, the matrix cracking pattern is essentially mechanically reproducible, with perhaps a certain statistical variation only. Wang *et al.* [26] and Fukunaga *et al.* [28] proposed a stochastic model for probability functions for flaw size and flaw distribution. In the present model, the cracks are assumed to instantly form across the entire cross section. In thick 90° plies the crack propagation is instantaneous across the entire cross section, but for thin 90° plies the microcrack formation can be partially suppressed [30]. Some recent finite element results show that the energy release rate is virtually independent of the length of the propagating microcrack in width direction [28, 29]. By this simplification it is possible to calculate the strain energy release rate by analysing the energy released due to the formation of a complete microcrack, where $2t_1 W$ is the fracture area of a single microcrack. We therefore simplify the microcrack damage problem by assuming that all microcracks instantaneously span the entire cross-section of the 90° plies, i.e. a through-the-width and through-the-thickness microcrack.

The energy release associated with the formation of a complete microcrack can be written as a function of the change in the strain energy (ΔU) of the structure and the total external work done (ΔU_{ext}), during formation of the crack for constant load or constant displacement conditions:

$$G_I = \left(\frac{\Delta U_{\text{ext}} - \Delta U}{2t_1 W} \right)_{P,u}. \tag{1}$$

We now postulate, as Parvizi *et al.* [30], that microcracks will form when the energy released due to the formation of the microcrack exceeds some critical value, i.e. the critical microcracking toughness of the material. It is now possible to calculate the energies in equation (1) and calculate the G_I from any approximate stress analysis.

3. THEORETICAL MODEL

An exact solution to a practical problem such as transverse cracking is almost impossible to obtain, but good approximate solutions give the qualitative features of the stress, strain and displacement fields. To solve the transverse cracking prob-

lem, a method based on the energy theorems of elasto-mechanics is applied. The Kantrovich method introduce the calculus of variations [22, 23].

An energy method which is simple to use, also for a three-dimensional cracking process such as in $[\pm\theta]$s lay-ups, and to use as the elastic solution in a numerical procedure for the viscoelastic damage predictions, in both cross-ply and angle-ply structures, is to assume a displacement field for the cracked structure. The complementary method is not used for several reasons. The most important is that for lay-ups other than cross-plies, difficulties arises because of the cumbersome nature of the complementary strain energy method, associated with assumed stress functions and traction boundary conditions. It is easier to satisfy the continuity and boundary conditions for a displacement field in a complex lay-up. Thus, a potential energy approach is chosen as the best tool for analysing both cross-ply and angle-ply structures. Aboudi [24] expanded the displacement field of a unit cell, representing a structure with aligned cracks, in Legendre polynomials, and used the minimum potential energy approach to calculate the effective elastic moduli. Aboudi's model gives approximately the same result as the shear-lag method, and requires higher order expansion of the assumed displacement to increase the accuracy of the model. Fang *et al.* [21] also used an assumed displacement field for the calculation of the thermal stresses in cracked cross-ply laminate. They used the same principles as Hashin, but derived a variational solution by minimising the potential energy. Aboudi used a two-dimensional field and Fang *et al.* used a one-dimensional field. All former energy methods approaches, both the complementary or the potential energy approaches, assume either a parabolic stress distribution in the layers or a parabolic crack opening displacement function, respectively. The current model assumes a displacement field consisting of only unknown functions, and by using the theorem of minimum potential energy under small admissible variations of the displacement field, an approximate solution for the strain field in the unit cell is found. Our model proposes a two-dimensional displacement field and, in addition, allows for the crack front displacement shape to be determined from the variational procedure. That implies the possibility of minimizing the potential energy with respect to the crack opening displacement function. A two-dimensional analysis is performed, but the third dimension enters by the assumption of plane stress, plane strain or generalised plane strain conditions. We describe a plane stress solution, but the plane strain or generalised plane strain solutions are trivially obtained by substituting the reduced mechanical properties of the plane stress solution. Consider a laminated composite structure built up by a number of 0° and 90° layers as illustrated in Fig. 1a. The marked area in this figure is taken as a representative element of the structure, and by use of symmetry considerations, the geometry shown in Fig. 1b represent the unit cell of the damaged material. Three load cases are to be considered. Figure 3a, b show the unit cell subjected to pure mechanical loads, an applied stress or displacement condition. The second load case is pure thermal loading Fig. 3c, d, and the third both thermal and mechanical loading.

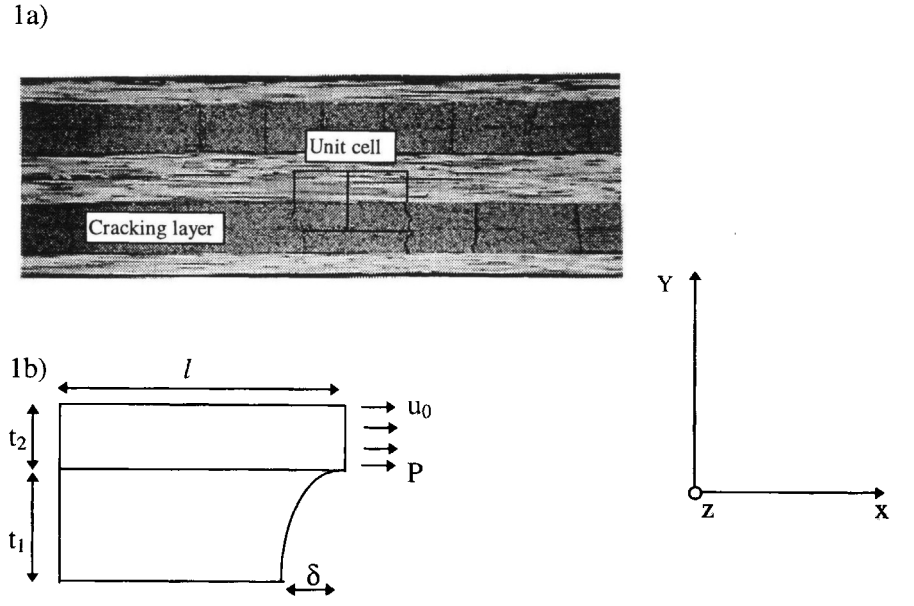

Figure 1. (a) Cross-section of a $[0, 90_2, 0]_s$ lay-up, showing transverse cracks in the off-axis layers. (b) The idealised unit cell.

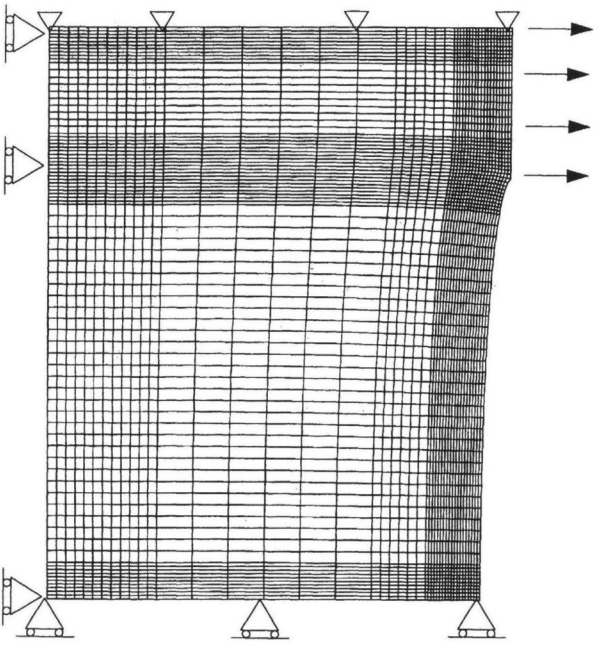

Figure 2. Displacement plot: deformed element mesh with boundary conditions.

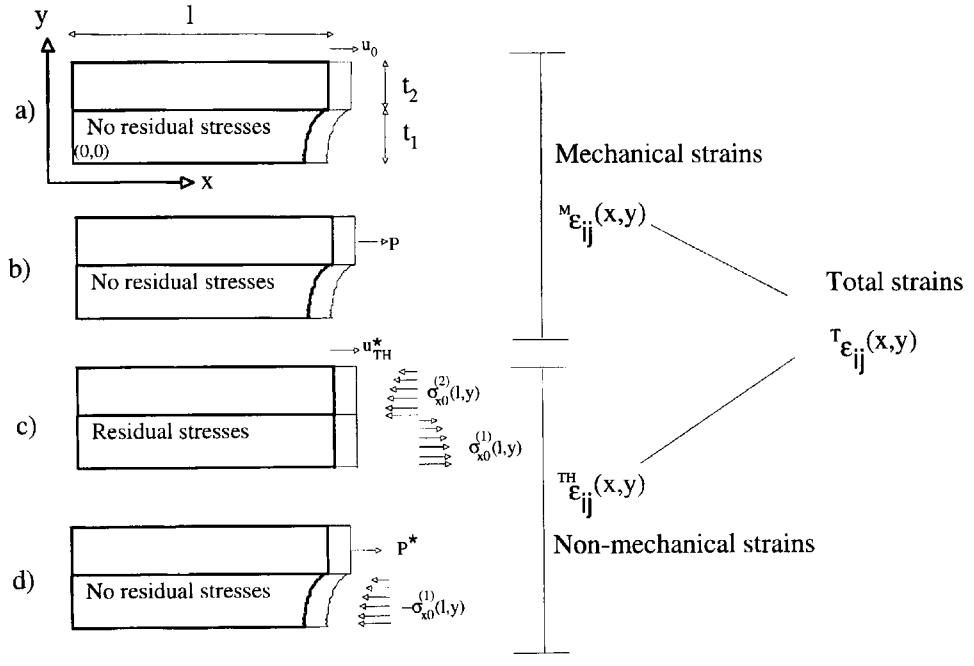

Figure 3. The unit cell subjected to three different load cases.

3.1. Mechanical loading

Assuming the xy-plane in Fig. 1b to remain plane, the displacement functions for each of the two layers in Fig. 1b may be assumed as equation (2):

$$\begin{aligned} u_x^{(1)}(x, y) &= f_1(x) + \phi(y) f_2(x), & u_x^{(2)}(x, y) &= f_1(x) + \phi(t_1) f_2(x), \\ u_y^{(1)}(x, y) &= \varepsilon_{y0}^{(1)} y, & u_y^{(2)}(x, y) &= \varepsilon_{y0}^{(1)} t_1 + \varepsilon_{y0}^{(2)}(y - t_1). \end{aligned} \tag{2}$$

The three unknown functions and the two unknown constants, are determined utilising the theorem of minimum potential energy. The $\phi(y)$-function describes the crack opening displacement, and must satisfy symmetry conditions on $y = 0$. It is assumed that linear elastic behaviour will prevail, and that all deformations can be considered small. For the geometry shown in Fig. 1, the boundary and continuity conditions for the displacement field are given by equation (3). The superscripts, (1), (2), refers to the cracked and uncracked layer, respectively.

$$\begin{aligned} u_x^{(1)}(0, y) &= 0, & u_x^{(1)}(x, t_1) &= u_x^{(2)}(x, t_1), \\ u_x^{(2)}(0, y) &= 0, & u_y^{(1)}(x, t_1) &= u_y^{(2)}(x, t_1), \\ u_y^{(1)}(x, 0) &= 0. \end{aligned} \tag{3}$$

The potential energy U for the unit cell is given in equation (4):

$$U = \frac{1}{2}\int_0^l \left(\int_0^{t_1} \left(\sigma_x^{(1)}\varepsilon_x^{(1)} + \sigma_y^{(1)}\varepsilon_y^{(1)} + \tau_{xy}^{(1)}\gamma_{xy}^{(1)}\right) \mathrm{d}y + \int_{t_1}^{t_2} \left(\sigma_x^{(2)}\varepsilon_x^{(2)} + \sigma_y^{(2)}\varepsilon_y^{(2)} + \tau_{xy}^{(2)}\gamma_{xy}^{(2)}\right) \mathrm{d}y \right) \mathrm{d}x - P u_x^{(2)}(l), \tag{4}$$

where the last term in equation (4) is the work done by the external force.

$$P = (t_1 + t_2) W \sigma_{\text{applied}}.$$

The out-of-plane dimension W is assumed to be unity. The stress/strain relations in the respective layers are given in equation (5):

$$\begin{aligned} \varepsilon_x &= \frac{\partial u_x}{\partial x}, & \sigma_x^{1,2} &= c_{11}^{1,2}\varepsilon_x^{1,2} + c_{12}^{1,2}\varepsilon_y^{1,2}, \\ \varepsilon_y &= \frac{\partial u_y}{\partial y}, & \sigma_y^{1,2} &= c_{12}^{1,2}\varepsilon_x^{1,2} + c_{22}^{1,2}\varepsilon_y^{1,2}, \\ \gamma_{xy} &= \frac{\partial u_x}{\partial y} + \frac{\partial u_y}{\partial x}, & \tau_{xy}^{1,2} &= c_{66}^{1,2}\gamma_{xy}^{1,2}, \end{aligned} \tag{5}$$

where $c_{11}^{1,2}, \ldots, c_{66}^{1,2}$ are the elastic stiffness coefficients.

The stress/strain relations inserted in equation (4) result in:

$$U = \frac{1}{2}\int_0^l \left\{ \int_0^{t_1} \left(c_{11}^{(1)}\left(\varepsilon_x^{(1)}\right)^2 + 2c_{12}^{(1)}\varepsilon_x^{(1)}\varepsilon_y^{(1)} + c_{22}^{(1)}\left(\varepsilon_y^{(1)}\right)^2 + c_{66}^{(1)}\left(\gamma_{xy}^{(1)}\right)^2\right) \mathrm{d}y + \int_{t_1}^{t_1+t_2} \left(c_{11}^{(2)}\left(\varepsilon_x^{(2)}\right)^2 + 2c_{12}^{(2)}\varepsilon_x^{(2)}\varepsilon_y^{(2)} + c_{22}^{(2)}\left(\varepsilon_y^{(2)}\right)^2 + c_{66}^{(2)}\left(\gamma_{xy}^{(2)}\right)^2\right) \mathrm{d}y \right\} \mathrm{d}x - P u_x^{(2)}(l). \tag{6}$$

We now give the displacement field a small variation so that the boundary conditions given by equation (3) are satisfied, i.e.:

$$\begin{aligned} u_x^{(1)} &\to u_x^{(1)} + \delta u_x^{(1)}, \\ u_x^{(2)} &\to u_x^{(2)} + \delta u_x^{(2)}, \\ \delta u_x^{(1)}(0, y) &= \delta u_x^{(2)}(0, y) = 0. \end{aligned} \tag{7}$$

The other conditions in equation (3) are automatically satisfied.

Among all admissible displacement variations δu_i (i.e. all variations that satisfy symmetry and boundary conditions and are continuous over the element and at its boundaries), the best approximation of the displacement field for the cross-section is distinguished by:

$$\delta U = 0. \tag{8}$$

The variation of the potential energy due to an arbitrary, but admissible variation of the displacement field is:

$$\begin{aligned}\delta U = \int_0^l \Bigg\{ \int_0^{t_1} \Big(& c_{11}^{(1)} \varepsilon_x^{(1)} \delta\varepsilon_x^{(1)} + c_{12}^{(1)} \big(\varepsilon_x^{(1)} \delta\varepsilon_y^{(1)} + \varepsilon_y^{(1)} \delta\varepsilon_x^{(1)}\big) + c_{22}^{(1)} \varepsilon_y^{(1)} \delta\varepsilon_y^{(1)} \\ & + c_{66}^{(1)} \gamma_{xy}^{(1)} \delta\gamma_{xy}^{(1)} \Big)\, \mathrm{d}y \\ + \int_{t_1}^{t_1+t_2} \Big(& c_{11}^{(2)} \varepsilon_x^{(2)} \delta\varepsilon_x^{(2)} + c_{12}^{(2)} \big(\varepsilon_x^{(2)} \delta\varepsilon_y^{(2)} + \varepsilon_y^{(2)} \delta\varepsilon_x^{(2)}\big) + c_{22}^{(2)} \varepsilon_y^{(2)} \delta\varepsilon_y^{(2)} \\ & + c_{66}^{(2)} \gamma_{xy}^{(2)} \delta\gamma_{xy}^{(2)} \Big)\, \mathrm{d}y \Bigg\}\, \mathrm{d}x - P \cdot \delta u_x^{(2)}(l).\end{aligned} \tag{9}$$

From equation (2) we obtain the strain components and their variations for the two layers:

$$\begin{aligned}
&\varepsilon_x^{(1)} = f_1'(x) + \phi(y) f_2'(x), && \varepsilon_x^{(2)} = f_1'(x) + \phi(t_1) f_2'(x), \\
&\delta\varepsilon_x^{(1)} = \delta f_1'(x) + \phi(y)\delta f_2'(x) && \delta\varepsilon_x^{(2)} = \delta f_1'(x) + \phi(t_1)\delta f_2'(x) \\
&\qquad + \delta\phi(y) f_2'(x), && \qquad + \delta\phi(t_1) f_2'(x), \\
&\varepsilon_y^{(1)} = \varepsilon_{y0}^{(1)}, \quad \delta\varepsilon_y^{(1)} = \delta\varepsilon_{y0}^{(1)}, && \varepsilon_y^{(2)} = \varepsilon_{y0}^{(2)}, \quad \delta\varepsilon_y^{(2)} = \delta\varepsilon_{y0}^{(2)}, \\
&\gamma_{xy}^{(1)} = \phi'(y) f_2(x), && \gamma_{xy}^{(2)} = 0, \quad \delta\gamma_{xy}^{(2)} = 0, \\
&\delta\gamma_{xy}^{(1)} = \phi'(y)\delta f_2(x) + \delta\phi'(y) f_2(x).
\end{aligned} \tag{10}$$

For the displacement and its variation at distance $x = l$ we have:

$$\begin{aligned}
u_x^{(2)}(l) &= f_1(l) + \phi(t_1) f_2(l), \\
\delta u_x^{(2)}(l) &= \delta f_1(l) + \phi(t_1)\delta f_2(l) + \delta\phi(t_1) f_2(l).
\end{aligned} \tag{11}$$

Inserting equations (10), (11) into equation (9), and performing the integration over the element volume gives a new expression for the variation of the potential energy. According to the boundary conditions in equation (3), we have:

$$f_1(0) = \delta f_1(0) = f_2(0) = \delta f_2(0) = 0. \tag{12}$$

The $\delta\phi(t_1)$ term in equation (11) will vanish because the results will show that $\phi(t_1)$ is constant, and its variation is therefore zero.

Thus, by this simplification, equation (9) can be written as:

$$\begin{aligned}\delta U = \int_0^l \Big(& -\big(\alpha_1 f_1''(x) + \alpha_2 f_2''(x)\big)\delta f_1(x) \\ & - \big(\alpha_2 f_1''(x) + \alpha_3 f_2''(x) - \alpha_4 f_2(x)\big)\delta f_2(x)\Big)\, \mathrm{d}x\end{aligned}$$

$$
\begin{aligned}
&+ \int_0^{t_1} \left(\left(\beta_1 + \beta_2 \phi(y) + \beta_3 \phi''(y) \right) \delta\phi(y) \right) \mathrm{d}y \\
&+ \left(\alpha_1 f_1'(l) + \alpha_2 f_2'(l) + \omega_1 \varepsilon_{y0}^{(1)} + \omega_2 \varepsilon_{y0}^{(2)} \right) \delta f_1(l) \\
&+ \left(\alpha_2 f_1'(l) + \alpha_3 f_2'(l) + \omega_3 \varepsilon_{y0}^{(1)} + \omega_4 \varepsilon_{y0}^{(2)} \right) \delta f_2(l) \\
&+ \left(\omega_1 f_1(l) + \omega_3 f_2(l) + \omega_5 \varepsilon_{y0}^{(1)} \right) \delta \varepsilon_{y0}^{(1)} \\
&+ \left(\omega_2 f_1(l) + \omega_4 f_2(l) + \omega_6 \varepsilon_{y0}^{(2)} \right) \delta \varepsilon_{y0}^{(2)} = 0,
\end{aligned}
\tag{13}
$$

where the constants $\alpha_1 - \omega_6$ (equation (14)) are dependent on the elements of the stiffness matrix for each layer, the geometry of the unit cell and on the crack opening displacement function.

$$
\begin{aligned}
&\alpha_1 = t_1 c_{11}^{(1)} + t_2 c_{11}^{(2)}, && && \omega_1 = c_{12}^{(1)} t_1, && \omega_5 = c_{22}^{(1)} t_1 l, \\
&\alpha_2 = c_{11}^{(1)} \textstyle\int_0^{t_1} \phi(y)\,\mathrm{d}y + t_2 \phi(t_1) c_{11}^{(2)}, && && \omega_2 = c_{12}^{(2)} t_2, && \omega_6 = c_{22}^{(2)} t_2 l, \\
&\alpha_3 = c_{11}^{(1)} \textstyle\int_0^{t_1} \left(\phi(y)\right)^2 \mathrm{d}y + t_2 \left(\phi(t_1)\right)^2 c_{11}^{(2)}, && && \omega_3 = c_{12}^{(1)} \textstyle\int_0^{t_1} \phi(y)\,\mathrm{d}y, \\
&\alpha_4 = c_{66}^{(1)} \textstyle\int_0^{t_1} \left(\phi'(y)\right)^2 \mathrm{d}y, && && \omega_4 = c_{12}^{(2)} t_2 \phi(t_1),
\end{aligned}
\tag{14}
$$

δU must equal zero for all combinations of $\delta f_1(x)$, $\delta f_2(x)$, $\delta \varepsilon_{y0}^{(1)}$, $\delta \varepsilon_{y0}^{(2)}$ and $\delta\phi(y)$. Hence from equation (13) we obtain the following set of equations, that must be solved in order to find the best approximation of the strain field. The governing differential equations are:

$$
\begin{aligned}
&\alpha_1 f_1''(x) + \alpha_2 f_2''(x) = 0, \\
&\alpha_2 f_1''(x) + \alpha_3 f_2''(x) - \alpha_4 f_2(x) = 0, \\
&\beta_3 \phi''(y) + \beta_2 \phi(y) + \beta_1 = 0,
\end{aligned}
\tag{15}
$$

where

$$
\begin{aligned}
&\beta_1 = c_{11}^{(1)} \textstyle\int_0^l f_1'(x) f_2'(x)\,\mathrm{d}x + \varepsilon_{y0}^{(1)} f_2(l) c_{12}^{(1)}, && \beta_2 = c_{11}^{(1)} \textstyle\int_0^l f_2'(x) f_2'(x)\,\mathrm{d}x, \\
&\beta_3 = -c_{66}^{(1)} \textstyle\int_0^l f_2'(x) f_2(x)\,\mathrm{d}x,
\end{aligned}
\tag{16}
$$

and the conditions:

$$
\begin{aligned}
&\alpha_1 f_1'(l) + \alpha_2 f_2'(l) + \omega_1 \varepsilon_{y0}^{(1)} + \omega_2 \varepsilon_{y0}^{(2)} = 0, && \text{(a)} \\
&\alpha_2 f_1'(l) + \alpha_3 f_2'(l) + \omega_3 \varepsilon_{y0}^{(1)} + \omega_4 \varepsilon_{y0}^{(2)} = 0, && \text{(b)} \\
&\omega_1 f_1(l) + \omega_3 f_2(l) + \omega_5 \varepsilon_{y0}^{(1)} = 0, && \text{(c)} \\
&\omega_2 f_1(l) + \omega_4 f_2(l) + \omega_6 \varepsilon_{y0}^{(2)} = 0, && \text{(d)}
\end{aligned}
\tag{17}
$$

are natural conditions connected to ϕ. This function should also obey the following conditions at $y = 0$, i.e.:

$$\phi(0) = 0, \qquad \phi'(0) = 0. \tag{18}$$

The two coupled second order differential equations give for the $f_1(x)$ and $f_2(x)$:

$$\begin{aligned} f_1(x) &= -\frac{\alpha_2}{\alpha_1}(A\cosh(\lambda_f x) + B\sinh(\lambda_f x)) + Cx + D, \\ f_2(x) &= A\cosh(\lambda_f x) + B\sinh(\lambda_f x). \end{aligned} \tag{19}$$

The solution of the second non-homogeneous differential equation for the crack opening displacement function is:

$$\phi(y) = A_\phi \sinh(\lambda_\phi y) + B_\phi \cosh(\lambda_\phi y) + C_\phi y + D_\phi. \tag{20}$$

The parameters λ_f and λ_ϕ in equations (19) and (20) are given by:

$$\lambda_f^2 = \frac{\alpha_4}{\alpha_3 - \dfrac{\alpha_2^2}{\alpha_1}} \geqslant 0, \qquad \lambda_\phi^2 = \frac{-\beta_2}{\beta_3} \geqslant 0. \tag{21}$$

The constants in equation (21) are given in equations (14) and (16). At $x = 0$, we have a plane of symmetry, so that the constants A and D must be equal to zero. Hence, the two f-functions are given by:

$$\begin{aligned} f_1(x) &= -\frac{\alpha_2}{\alpha_1}(B\sinh(\lambda_f x)) + Cx, \\ f_2(x) &= B\sinh(\lambda_f x). \end{aligned} \tag{22}$$

Note that Cx is the displacement function for the uniaxial case without cracks. The function $f_1(x)$ can be written as:

$$f_1(x) = -\frac{\alpha_2}{\alpha_1} f_2(x) + Cx. \tag{23}$$

The function $f_2(x)$ can then be interpreted as a disturbing function, which describes the effect of the crack at $x = l$.

The solution for $\phi(y)$ is obtained by the necessary boundary conditions due to symmetry at $y = 0$, and that the slope of the function is zero at the symmetry line.

$$\phi(y) = \frac{\Psi_\phi}{\lambda_\phi^2}(\cosh(\lambda_\phi y) - 1). \tag{24}$$

The constant Ψ_ϕ in the expression for the crack opening displacement function is already taken into account in $f_1(x)$ and $f_2(x)$, so the correct shape function is:

$$\phi(y) = (\cosh(\lambda_\phi y) - 1). \tag{25}$$

By inserting the solutions of the differential equations in equation (21), it is found that $\lambda_f = F(\lambda_\phi)$ and $\lambda_\phi = G(\lambda_f)$ are pure functions of λ_ϕ and λ_f, respectively. Thus it is possible to solve the relation $\lambda_f = F(G(\lambda_f))$ by a simple Newton–Raphson procedure. The parameters λ_f and λ_ϕ in equations (16), (17) are solved, and the solution is complete. Equation (21) shows that the parameters λ_f and λ_ϕ are dependent on the length of the unit cell, i.e. the crack front shape function changes as a function of crack density.

The obtained strain field is now used to find the total strain energy due to an applied stress $P/(t_1+t_2)$ at $x = l$. The strain energy is given in Fig. 10 together with numeric solutions. The results show a decrease in normalized strain energy towards a limit (no load bearing capacity in the cracking layer) as the damage increases. The solution scheme is easily modified to an applied strain condition (displacement controlled test). All terms containing P vanish, and the natural conditions (c) and (d) in equation (17) are unchanged.

The boundary condition at $x = l$ and its variation gives:

$$\begin{aligned} &u_x^{(2)}(l) = f_1(l) + \phi(t_1) f_2(l) = u_0, \\ &\delta u_x^{(2)}(l) = \delta f_1(l) + \delta\phi(t_1) f_2(l) + \phi(t_1)\delta f_2(l) = \delta u_0 = 0, \\ &\delta f_1(l) = -\phi(t_1)\delta f_2(l). \end{aligned} \tag{26}$$

Equation (26) couples the natural boundary conditions (a) and (b) in equation (17), and leads to a new natural boundary condition:

$$\begin{aligned} &(\alpha_2 - \phi(t_1)\alpha_1) f_1'(l) + (\alpha_3 - \phi(t_1)\alpha_2) f_2'(l) \\ &\quad + (\omega_3 - \phi(t_1)\omega_1)\varepsilon_{y0}^{(1)} + (\omega_4 - \phi(t_1)\omega_2)\varepsilon_{y0}^{(2)} = 0. \end{aligned} \tag{27}$$

Thus for an prescribed strain condition, equations (26), (27) and equations (17) c, d are used instead of equations (17) a, b, c, d. The differential equations are unchanged.

3.2. *Thermal load solution*

Assume the laminate to be stress free at temperature T_{ref}, and let ΔT denote the temperature change to a lower temperature level T_0. Due to the mismatch between the longitudinal and transverse coefficient of thermal expansion, residual stresses will build up in each ply, and deform the laminate depending on ΔT. When the temperature change is sufficiently large, microcracks will form in the laminate because of the thermal stress field. The cracking process will relieve some of the thermal stresses, and induce additional deformations of the laminate. Thus, for a constant temperature change, the displacement at $x = l$ (u_{TH}^* in Fig. 3c), will change as a function of crack density, i.e. the longitudinal coefficient of thermal expansion is a function of crack density.

To account for the residual stresses, due to cooling from the stress-free temperature, a separate analysis must be carried out. The solution procedure is the same

as for the pure mechanical load case, but the boundary conditions are changed. Let us assume for the uncracked structure, that residual stresses, independent of y, are present in both layers. An initial strain field ${}^{TH}_{0}\varepsilon_{ij}(x, y)$ depending on ΔT, is created, as shown in Fig. 3c. By introducing a crack, a stress-free surface is introduced in the structure. To simulate the cracking process, two load cases must be solved. We now set $\Delta T = 0$, i.e. no residual stresses are present in the structure. The initial residual stress ${}^{\text{res}}\sigma^{(1)}_{x0}$ is then applied to the crack surface at $x = l$, as a mechanical load, together with a stress of opposite sign ${}^{\text{res}}\sigma^{(2)}_{x0}$ acting on the uncracked layer, to provide the force equilibrium for the cross section at $x = l$ (see Fig. 3d). (Thermal loads create no resultant forces, when no restraints are acting on the structure.) Thus, a strain field ${}^{TH}_{(\sigma_{\text{res}})}\varepsilon_{ij}(x, y)$ due to the residual stresses applied at the boundary $x = l$ is obtained. The superposition of the strain fields for the two load cases above give the resultant strain field for the cracked structure subjected to pure thermal loading.

$$ {}^{TH}_{0}\varepsilon_{ij} + {}^{TH}_{(\sigma_{res})}\varepsilon_{ij} = {}^{TH}_{l}\varepsilon_{ij}. \tag{28} $$

To provide a general solution for the thermal cracking strain field, let us assume a structure ($l = l_0$) with a crack at $x = l_0$. For a cracked structure, the residual stresses are no longer uniform through the thickness. The reduced non-uniform residual stresses are calculated at the initiation point for the next crack, i.e. at $x = 0$. We now introduce a crack at $x = 0$, and let these stresses act on the crack surface, at $x = l$, for the new structure ($l = l_0/2$). In the expression for the potential energy, the work done by the residual stresses acting on the boundaries at $x = l$ must be taken into account. Thus, the potential energy can be written as:

$$ \begin{aligned} U = \frac{1}{2}\int_0^l \Bigg\{ \int_0^{t_1} \Big(& c^{(1)}_{11}\big(\varepsilon^{(1)}_x\big)^2 + 2c^{(1)}_{12}\varepsilon^{(1)}_x\varepsilon^{(1)}_y + c^{(1)}_{22}\big(\varepsilon^{(1)}_y\big)^2 + c^{(1)}_{66}\big(\gamma^{(1)}_{xy}\big)^2 \Big)\,\mathrm{d}y \\ & + \int_{t_1}^{t_2} \Big(c^{(2)}_{11}\big(\varepsilon^{(2)}_x\big)^2 + 2c^{(2)}_{12}\varepsilon^{(2)}_x\varepsilon^{(2)}_y + c^{(2)}_{22}\big(\varepsilon^{(2)}_y\big)^2 \\ & \qquad + c^{(2)}_{66}\big(\gamma^{(2)}_{xy}\big)^2 \Big)\,\mathrm{d}y \Bigg\}\,\mathrm{d}x \\ & - \int_0^{t_1} \sigma^{(1)}_{x0}(0, y)u^{(1)}_x(l, y)\,\mathrm{d}y - \int_{t_1}^{t_1+t_2} \sigma^{(2)}_{x0}(0, y)u^{(2)}_x(l, y)\,\mathrm{d}y. \end{aligned} \tag{29} $$

By minimising the potential energy with respect to the unknown functions, $f_1(x)$, $f_2(x)$, $\varepsilon^{(1)}_{y0}$, $\varepsilon^{(2)}_{y0}$ and $\phi(y)$ we obtain an approximate solution for the strain field due to the non-uniform residual stresses at $x = l$. By superposition of this strain field and the strain field obtained from the previous damage state, the total strain field is obtained. By inserting this thermal strain field, referred to as ${}^{TH}\varepsilon_{ij}(x, y)$, into the potential energy, the strain energy U_{res} due to a temperature change is obtained. The thermal strain energy as a function of crack density is given

in Fig. 11. As expected, the strain energy will decrease rapidly to zero as the damage increases.

3.3. The combined mechanical and thermal loading

The total strain energy for the combined load case is found by superposition of the two subsolutions (a + c + d) — (displacement controlled), or (b + c + d) — (load controlled) in Fig. 3, i.e. the sum of mechanical and thermal strains.

$$^{T}\varepsilon_{ij} = {}^{TH}\varepsilon_{ij} + {}^{M}\varepsilon_{ij}. \tag{30}$$

In a linear elastic analysis, the strains are additive, but the strain energies are not. The updated strain field in equation (30), is used to calculate the total strain energy of the unit cell, including the presence of residual stresses. The expression for the elastic strain energy is written in terms of the updated strain field:

$$U = \int_V \frac{1}{2} c_{ijklj}\left({}^{TH}\varepsilon_{ij} + {}^{M}\varepsilon_{ij}\right)\left({}^{TH}\varepsilon_{kl} + {}^{M}\varepsilon_{kl}\right) \mathrm{d}V. \tag{31}$$

Thus two sub-analyses must be performed to account for the residual stresses.

The total force P^* in load case d in Fig. 3 is given by equation (32) and the sum of the stresses at the boundary must be equal but of opposite sign in the two layers.

$$P^* = \int_0^{t_1} \sigma_{x0}^{(1)}(l, y)\,\mathrm{d}y = \int_{t_1}^{t_1+t_2} \sigma_{x0}^{(2)}(l, y)\,\mathrm{d}y. \tag{32}$$

4. FRACTURE CRITERIA

The determination of the strain field and the respective strain energy in the section above can be used for a linear elastic fracture mechanics (LEFM) based criterion for damage development. The energy of the unit cell, for increasing applied stress or strain, at different crack densities, can be calculated resulting in the curve spectrum in Fig. 8. The upper and lower limits can be looked upon as the uncracked response, and the saturation limit response. For the first damage state, a change in the energy ΔU_0 is observed, i.e. the energy required to create the crack surface $2t_1 W$. By the energy approach, the microcrack will form when the energy release rate on forming that microcrack reaches the critical energy release rate, or the microcracking fracture toughness for the material system. According to the assumption of equally spaced cracks, the next damage state will form when the possible energy released reaches ΔU_0. Cracks are allowed to form until there is not enough stored to create new crack surfaces.

5. RESULTS AND DISCUSSION

In this section we define the effective modulus for the cracked laminate, as a function of crack density. The effective modulus is equivalent to the net stress

Table 1.
Material properties of the two composite systems*

Reduced stiffness	Glass/epoxy	AS-4-3502
Layer 1:		
c_{11}	15784.4	11631.8
c_{22}	15784.4	11631.8
c_{12}	6629.4	4884.3
c_{66}	4580	4200
Layer 2:		
c_{11}	42903.8	145660
c_{22}	15784.4	11631.8
c_{12}	4012.6	2891.1
c_{66}	3400	4790
G_{IC}	250 J/m^2	
Layer thickness	0.203 mm	0.127 mm

* The values are taken from [1, 19].

divided by the average strain $\bar{\varepsilon}_x^{(2)}$ in the uncracked plies. All the results are derived from a displacement controlled condition, i.e. a forced displacement at $x = l$. The net stress $\bar{\sigma}_x$ can be expressed as:

$$\frac{\int_0^{t_1} \sigma_x^{(1)}(0, y)\,\mathrm{d}y + \int_{t_1}^{t_1+t_2} \sigma_x^{(2)}(0, y)\,\mathrm{d}y}{t_1 + t_2} = \bar{\sigma}_x, \tag{33}$$

thus the effective modulus:

$$\frac{\bar{\sigma}_x}{\bar{\varepsilon}_x^{(2)}} = E_x. \tag{34}$$

By inserting the solution for the strain field in equation (5), and normalise the axial modulus by the modulus of the uncracked structure, the stiffness degradation can be written as:

$$\frac{E_x}{E_{x0}} = \frac{l\Psi_1\left[\lambda_f \cosh(\lambda_f l)((\cosh(\lambda_\phi t_1) - \Psi_2)\right] - \Psi_3 l}{E_{x0} u_0}, \tag{35}$$

where

$$\Psi_1 = c_{11}^{(2)} B, \quad \Psi_2 = 1 + \frac{\alpha_2}{\alpha_1}, \quad \Psi_3 = c_{11}^{(2)} C + c_{12}^{(2)} \varepsilon_{0y}^{(2)}. \tag{36}$$

The modulus degradation for glass fibre/epoxy and carbon fibre/epoxy is shown in Figs 4–7, where the present model is compared to the shear lag predictions, and the lower bound predictions given by Hashin's model. In addition to the analytical solution, several finite element analyses were carried out, to verify the predictions in the analytical solution. The finite element model is depicted in Fig. 2. To predict the stiffness decrease, only the mechanical load case has to be solved. This is because the residual stresses make no contribution to the resultant stress due to a mechanical

load case. A similar prediction of the axial coefficient of thermal expansion can be made by examining the average strain in the uncracked layer due to a thermal load ΔT:

$$\alpha_x \Delta T l = u_x^{(2)}(l, t_1),$$
$$\frac{\alpha_x}{\alpha_{x0}} = \frac{\frac{B}{l}(\cosh(\lambda_\phi t_1) - \Psi_2)\sinh(\lambda_f l) + C}{\Delta T l \alpha_{x0}}. \tag{37}$$

In all lay-ups, the present model predictions were between Hashin's lower bound solution, and the shear-lag model. The finite element solution and the model have the largest discrepancies, when the thickness ratio of the two plies t_2/t_1, and the relative stiffness $E_x^{(1)}/E_x^{(2)}$ between the two layers are small. Thus, the model predicts the stiffness decrease for all the carbon fibre laminates very well, compared to the experimental data, and the finite element solution is close to the predictions. For the glass fibre/epoxy experimental data given by Highsmith and Reifsnider [1], there are discrepancies between Hashin's and our model. The present model assumes a uniform displacement of $u_x^{(2)}(x, t_1 + t_2)$, which is more correct for a stiff uncracked layer, such as carbon fibre/epoxy, and less correct for the softer glass fibre/epoxy outer layer. The crack density *vs* applied stress data in Fig. 9 give rise to speculations because, between 150 and 300 MPa, only a small change in crack density is observed, and the curve levels off quite early at a crack density of 0.8. Generally, the crack growth curve may be influenced by other modes of failure which emerge at higher load levels. For experimental values of the stiffness decrease and crack densities *vs* applied stress, the effect of other failure modes can be quite significant. Interlaminar delaminations can give rise to large decreases in stiffness, leading to an overestimation by the analytical models, of the stiffness decrease. Also, the delamination process increases the intermediate crack length leading to a CDS different from the analytical CDS. Thus, the stiffness decrease at high load levels can be higher than expected from pure matrix cracking, which can explain the perfect fit of the lower bound solution and the experimental data in Fig. 9. Other failure modes such as delaminations are not taken into account in our or Hashin's approach. The crack density as a function of applied stress given from the model lies between the almost identical predictions of Hashin and Varna and the predictions of the shear-lag model. The value of $G_I = 250$ J/m^2 is given by Highsmith and Reifsnider [1], but one can discuss the accuracy of this value. The material 'parameter' ΔU_0 can be assigned to fit the first crack or to fit the steep part of the experimental curve. To provide accurate values of ΔU_0 one must find the value ΔU_0, which gives the overall best fit for data obtained from tests on different thickness ratios of the layers and load levels, to provide the characteristic damage state for each lay-up.

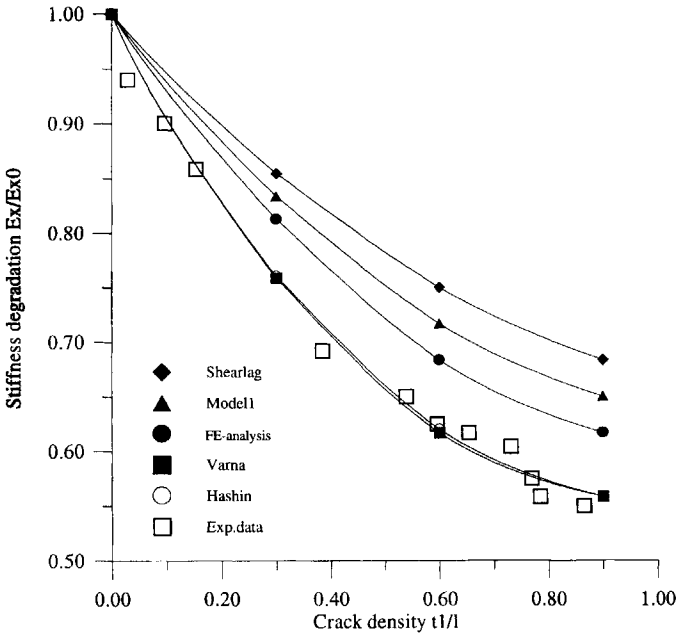

Figure 4. Stiffness degradation as a function of crack density for a glass fibre/epoxy $[0/90_3]_S$ lay-up (data taken from [1]).

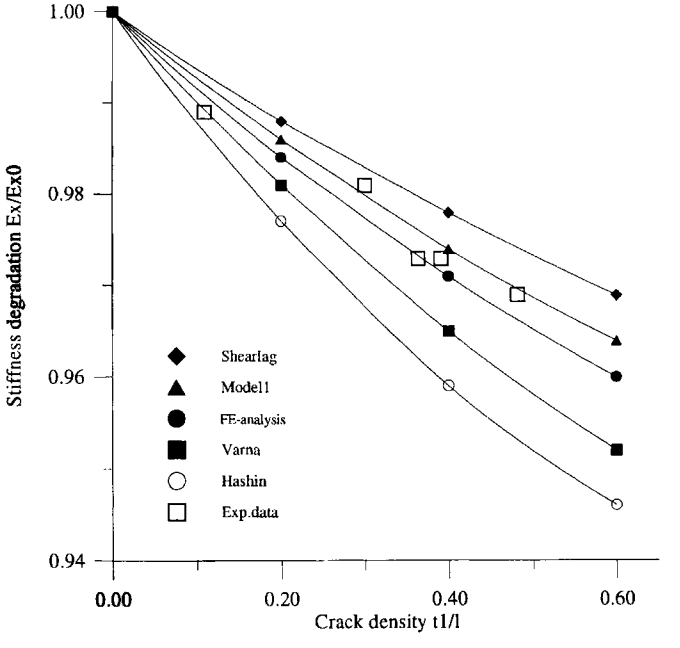

Figure 5. Stiffness degradation as a function of crack density for a carbon AS4/epoxy $[0/90_2/0]_T$ lay-up (data taken from [19]).

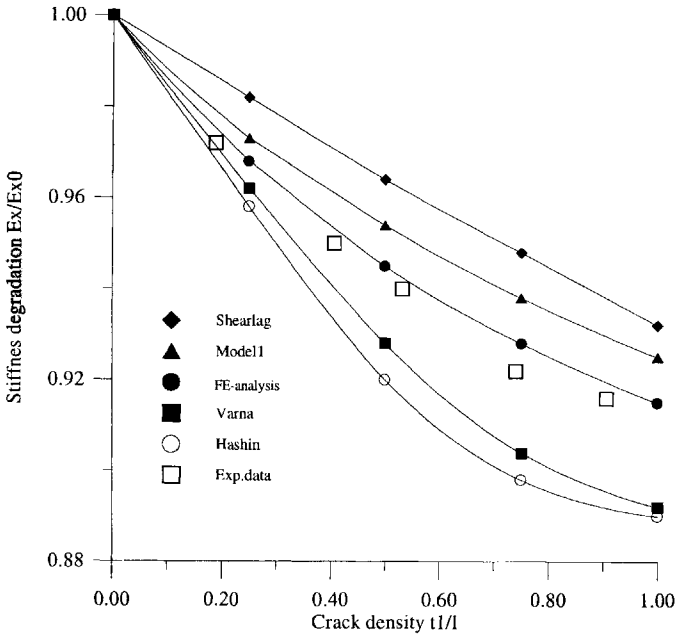

Figure 6. Stiffness degradation as a function of crack density for a carbon AS4/epoxy $[0/90_4/0]_T$ lay-up (data taken from [19]).

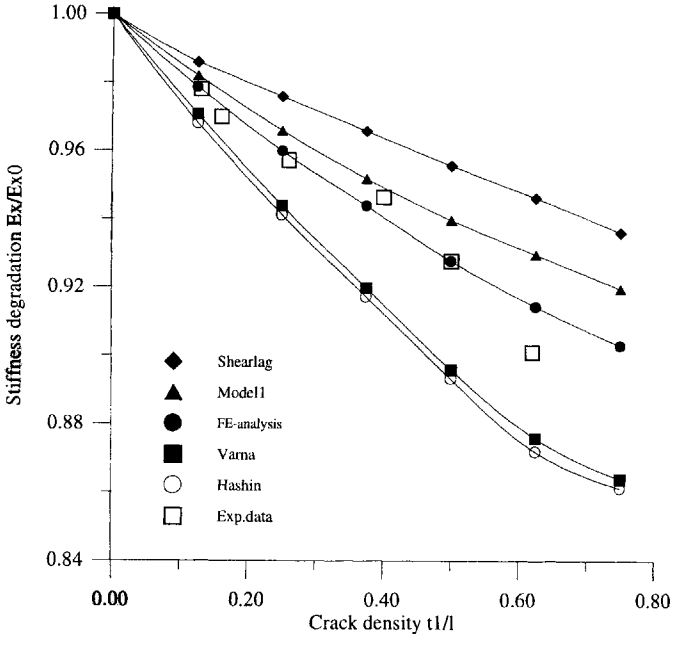

Figure 7. Stiffness degradation as a function of crack density for a carbon AS4/epoxy $[0/90_6/0]_T$ lay-up (data taken from [19]).

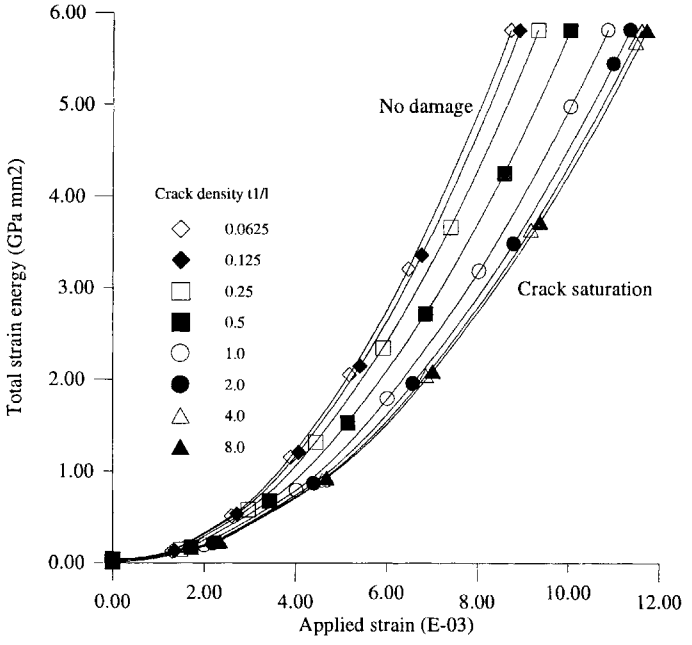

Figure 8. Total strain energy [GPa mm^2 $\times$ 10^{-3}] *vs* applied strain for different damage states.

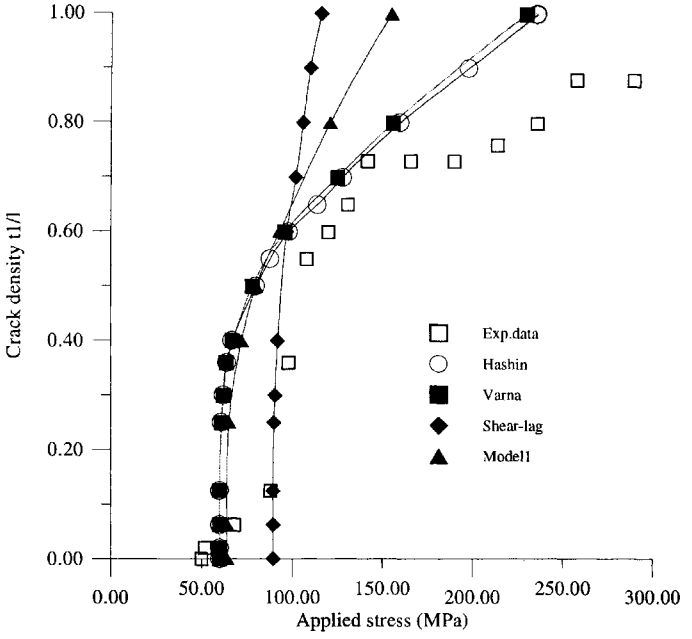

Figure 9. Crack density as a function of applied stress.

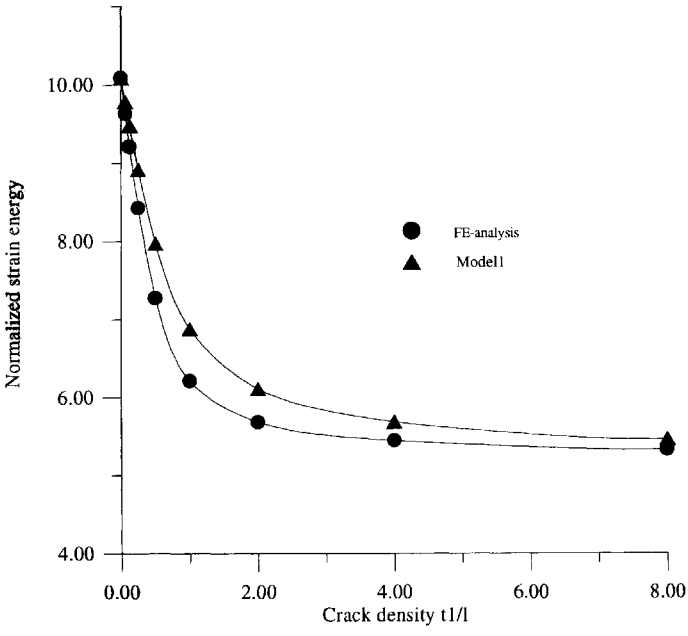

Figure 10. Normalized strain energy [GPa/$(l(t_1 + t_2)\varepsilon_x^2)$] due to pure mechanical loading.

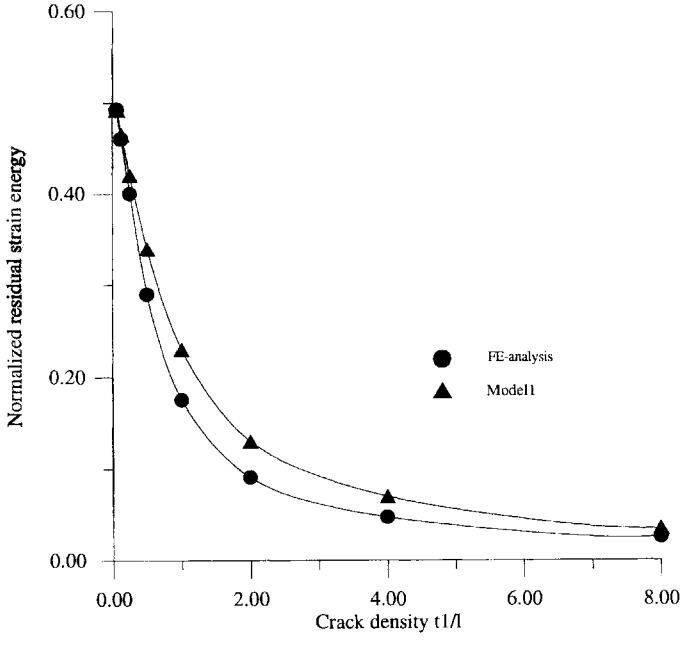

Figure 11. Normalized residual strain energy [GPa · $\varepsilon_x^2/(l(t_1 + t_2))$] due to pure thermal loading.

6. CONCLUSION

The main goal for this paper was to develop a model for the strain and stress field in the region between two cracks in a cross-ply structure in tensile loading. The validity of the current model was investigated by comparing the stiffness reduction, as a function of crack density, given by the model and by numerical finite element results. Existing models such as Hashin's complementary energy approach were also compared to the our results. The current model assumes a displacement field, thus an upper bound solution, by minimising the potential energy. The crack front shape is allowed to deform freely, making it possible to minimise the strain energy with respect to the crack opening displacement function. The current model predictions are always between the shear-lag model and the lower bound solutions. For very large thickness ratio of the two plies t_2/t_1 and large relative stiffness $E_x^{(1)}/E_x^{(2)}$, the present model underestimates the stiffness decrease for the glass fibre/epoxy data, but shows excellent fit for all the carbon fibre lay-ups. This method has also been used to predict three-dimensional cracking, such as in $[\pm\theta]$s-lay-ups, showing very good correlation between stiffness decrease measurements on angle-ply filament wound pipes, and 3D-model predictions.

REFERENCES

1. A. L. Highsmith and K. L. Reifsnider, Stiffness reduction mechanisms in composite laminates, in: *Damage in Composites Materials, ASTM STP 775*, K. L. Reifsnider (Ed.), pp. 103–117. ASTM, Philadelphia, PA (1982).
2. D. S. Adams and C. T. Herakovich, Influence of damage on the thermal response of graphite/epoxy laminates, *J. Thermal Stresses* **7**, 91–113 (1984).
3. M. G. Bader, J. E. Bailey, P. T. Curtis and A. Parvizi, The mechanism of initiation and development of damage in multi-axial fiber reinforced plastics laminates, mechanical behaviour of materials, in: *Proc. 3rd Intern. Conf.*, Cambridge, England, pp. 227–239 (1979).
4. K. L. Reifsnider, Some fundamental aspects of the fatigue and fracture response of composite materials, in: *Proc. 14th Ann. Meeting of Soc. Engng Sci.*, pp. 343–384. Bethlehem, PA (1977).
5. K. W. Garret and J. E. Bailey, Multiple transverse fracture in 90° cross-ply laminates of a glass fibre reinforced polyester, *J. Mater. Sci.* **12**, 157–168 (1977).
6. F. W. Crossman and A. S. D. Wang, The dependence of transverse cracking and delamination on ply thickness in graphite-epoxy laminates, in: *Damage in Composite Materials, ASTM STP 775*, K. L. Reifsnider (Ed.), pp. 40–62. ASTM, Philadelphia, PA (1982).
7. A. S. D. Wang, Characterization, analysis and significance of defect in composite materials, Fracture mechanics of sublaminate, Cracks in composite laminates, in: *AGARD CP 355*, pp. 15.1–15.19 (1983).
8. R. Talreja, Transverse cracking and stiffness reduction in composite laminates, *J. Compos. Mater.* **19**, 335–375 (1985).
9. W.-L. Jong, D. H. Allen and C. E. Harris, Internal state variable approach for predicting stiffness reductions in fibrous laminated composites with matrix cracks, *J. Compos. Mater.* **23**, 1273–1291 (1989).
10. J. Renard and A. Thionnet, A meso-macro approach to predict the damage evolution of transverse cracking in laminated composite, in: *Damage Mechanics in Composites*, Vol. 32, pp. 31–39. ASME (1992).

11. N. Laws and G. J. Dvorak, Progressive transverse cracking in composite laminates, *J. Compos. Mater.* **22**, 900–915 (1988).
12. S. R. Swanson, On the mechanics of microcracking in fiber composite laminates under combined stress, *J. Engng Mater. Technol., Trans. ASME* **111**, 145–149 (1989).
13. D. L. Flaggs, Prediction of tensile matrix failure in composite laminates, *J. Compos. Mater.* **19**, 29–50 (1985).
14. C. L. Tsai and I. M. Daniel, The behaviour of cracked cross ply composite laminates under general in-plane loading, in: *Damage in Composite Materials*, G. Z. Voyiadjis (Ed.), pp. 51–66. Elsevier, Amsterdam (1993).
15. Z. Hashin, in: *Analysis of Cracked Laminates: A Variational Approach, Mechan. Mater.*, Vol. 4, pp. 121–136. North-Holland (1985).
16. Z. Hashin, Analysis of stiffness reduction of cracked cross-ply laminates, *Engng Fract. Mech.* **25**, 771–778 (1986).
17. J. A. Nairn, The strain energy release rate of composite microcracking: A variational approach, *J. Compos. Mater.* **23**, 1106–1129 (1989).
18. S. Liu and J. A. Nairn, The formation and propagation of matrix microcracks in cross-ply laminates during static loading, *J. Reinf. Plast. Compos.* **11**, 158–178 (1992).
19. J. Varna, Analysis of transverse cracking in composite cross-ply laminates, Doctoral thesis, Luleå Univ. of Technology, Sweden (1992).
20. J. A. Nairn and S. Hu, in: *Matrix Microcracking: Damage Mechanics of Composite Materials*, R. Talreja (Ed.), pp. 187–243. Elsevier, Amsterdam (1994).
21. G. P. Fang, R. A. Schapery and Y. Weitsman, Thermally-induced fracture in composites, *Engng Fract. Mech.* **33** (4), 619–632 (1989).
22. Y. C. Fung, *Foundations of Solid Mechanics*. Prentice Hall (1965).
23. F. B. Hildebrand, *Methods of Applied Mathematics*, 2nd edn. Prentice Hall (1965).
24. J. Aboudi, Stiffness reduction of cracked solids, *Engng Fract. Mech.* **26**(5), 637–650 (1987).
25. J. Varna and L. A. Berglund, Multiple transverse cracking and stiffness reduction in cross-ply laminates, *J. Compos. Technol. Res.* **13**, 97–106 (1991).
26. A. S. D. Wang, P. C. Chou and S. C. Lei, A stochastic model for the growth of matrix cracks in composite laminates, *J. Compos. Mater.* **18**, 239–254 (1984).
27. H. Fukunaga and T.-W. Chou, Probabilistic failure strength analysis of graphite/epoxy cross-ply laminates, *J. Compos. Mater.* **18**, 339–356 (1984).
28. F. J. Guild, S. L. Ogin and P. A. Smith, Modelling of 90° ply cracking in cross ply laminates, including three dimensional effects, *J. Compos. Mater.* **27**, 646–667 (1993).
29. W. Binienda, A. Hong and G. D. Robbers, Influence of material parameters on strain energy release rates for cross-ply laminates with a pre-existing transverse crack, *Compos. Engng* **4** (12), 1197–1210 (1994).
30. A. Parvizi, K. W. Garret and J. E. Bailey, Constrained cracking in glass fiber reinforced epoxy cross-ply laminates, *J. Mater. Sci.* **13**, 195–201 (1978).
31. ANSYS rev.5.1, Swanson Analysis Systems Inc., Houston (1994).
32. R. Anderssen, P. A. Gradin, C.-G. Gustafson and P. Nygård, Prediction of crack development and stiffness degradation in angle-ply filament wound pipes, in: *ICCM-10*, pp. 407–414 (1995).